A Journal of the Gesellschaft Deutscher Chemiker

Angewandte International Edition GDCh Chemie

www.angewandte.org

Accepted Article

Title: Sub-3 nm Ultrafine Cu2O for Visible Light-driven Nitrogen Fixation

Authors: Shuai Zhang, Yunxuan Zhao, Run Shi, Chao Zhou, Geoffrey I.N. Waterhouse, Zhuan Wang, Yuxiang Weng, and Tierui Zhang

To be cited as: *Angew. Chem. Int. Ed.* 10.1002/anie.202013594

Link to VoR: https://doi.org/10.1002/anie.202013594

WILEY-VCH

10.1002/anie.202013594

WILEY-VCH

RESEARCH ARTICLE

Sub-3 nm Ultrafine Cu_2O for Visible Light-driven Nitrogen Fixation

Shuai Zhang,[a, b] Yunxuan Zhao,*[a] Run Shi,[a] Chao Zhou,[a] Geoffrey I.N. Waterhouse,[c] Zhuan Wang,[d] Yuxiang Weng,[d, e, f] and Tierui Zhang*[a, b]

[a] S. Zhang, Dr. Y. Zhao, Dr. R. Shi, Dr. C. Zhou, Prof. T. Zhang
Key Laboratory of Photochemical Conversion and Optoelectronic Materials
Technical Institute of Physics and Chemistry, Chinese Academy of Sciences
Beijing, 100190 (China)
E-mail: tierui@mail.ipc.ac.cn; yunxuan@mail.ipc.ac.cn
[b] S. Zhang, Prof. T. Zhang
Center of Materials Science and Optoelectronics Engineering
University of Chinese Academy of Sciences
Beijing, 100049 (China)
[c] Prof. G. I.N. Waterhouse
School of Chemical Sciences
The University of Auckland
Auckland, 1142 (New Zealand)
[d] Dr. Z. Wang, Prof. Y. Weng
Beijing National Laboratory for Condensed Matter Physics, Laboratory of Soft Matter Physics
Institute of Physics, Chinese Academy of Sciences
Beijing, 100190 (China)
[e] Prof. Y. Weng
School of Physical Sciences
University of Chinese Academy of Sciences
Beijing, 100049 (China)
[f] Prof. Y. Weng
Songshan Lake Materials Laboratory
Dongguan, Guangdong, 523808 (China)

Supporting information for this article is given via a link at the end of the document.

Abstract: Photocatalytic N_2 fixation to NH_3 with water as the reducing agent represents a promising future strategy for ammonia synthesis, motivating the discovery of efficient photocatalysts that offer high sunlight utilization and catalytic efficiency to N_2 fixation. Cu_2O, a low-cost, visible light-responsive semiconductor photocatalyst represents an ideal candidate for visible light-driven photocatalytic reduction of N_2 to NH_3 from the viewpoint of thermodynamics, but remaining unexplored in this field yet. Noticeably, a majority of Cu_2O photocatalysts synthesized to date with large lateral sizes (typically tens to hundreds of nanometers) generally suffer from severe electron-hole recombination and limited surface sites, restricting its photocatalytic activity for potential N_2 fixation. Ultrafine photocatalysts with lateral dimensions ~1-3 nm offer distinct advantages over conventional nanoparticle-based photocatalysts in this context, though the controlled synthesis of ultrafine photocatalysts remains challenging. Herein, we report the successful synthesis of uniformly sized and ultrafine Cu_2O platelets with lateral size < 3 nm *via* the *in-situ* topotactic reduction of a Cu(II)-containing layered double hydroxide with ascorbic acid. The supported ultrafine Cu_2O offered excellent performance and stability for the visible light-driven photocatalytic reduction of N_2 to NH_3 (the Cu_2O-mass-normalized rate as high as 4.10 mmol $g_{Cu_2O}^{-1}$ h^{-1} at λ > 400 nm), with the origin of the high activity being long-lived photo-excited electrons in trap states, an abundance of exposed active sites and the underlying support structure. This work guides the future design of ultrafine catalysts for NH_3 synthesis and other applications.

Introduction

The catalytic reduction of nitrogen (N_2) to ammonia (NH_3) represents one of the most important industrial processes in today's chemical industry, with the NH_3 produced being an indispensable feedstock for the synthesis of nitrogen-based fertilizers and various commodity chemicals.[1] In recent years, the photocatalytic N_2 reduction reaction (pNRR) has emerged as an exciting new research field, harnessing renewable solar energy and a semiconductor photocatalyst to drive the chemical reaction of N_2 to NH_3 using H_2O as a proton source. Such an approach is desirable from a green chemistry perspective relative to the incumbent and energy-intensive Haber-Bosch process.[2] However, N≡N triple bonds are extremely strong (941 kJ mol^{-1}), making the kinetics of pNRR too slow to demand serious industry interest at the present time. In order to improve pNRR kinetics, efficient N_2 activation on the surface of photocatalysts and fast transfer of energetic electrons to adsorbed N_2 are demanded.[3] Generally, the limited availability of active sites on the surface of photocatalysts for N_2 adsorption is rate-limiting.[4] Electron-hole pair recombination in the semiconductor photocatalyst also limits the availability of electrons and holes for N_2 reduction and H_2O oxidation, respectively, on the surface of the photocatalyst.[5] These two issues are current bottlenecks to efficient pNRR, motivating the search for new photocatalysts or strategies for circumventing these bottlenecks.

10.1002/anie.202013594

Copper oxides due to their multi-electron transfer properties show great promise in solar energy conversion and heterogeneous photocatalysis.[6] Cuprous oxide (Cu_2O) is a low-cost and visible light-responsive material, already finding widespread application in photoelectrochemical/photocatalytic conversion processes.[7] Cu_2O possesses appropriate conduction and valence band level for driving N_2 reduction and water oxidation, respectively, making it a near-ideal candidate for visible light-driven photocatalytic reduction of N_2 to NH_3 in pure water. However, to our knowledge, no prior work examining the photocatalytic performance of Cu_2O for N_2 reduction, motivating an exciting attempt and a detailed investigation. It is worth noting that although the intrinsic properties of Cu_2O make it very suitable as a NRR photocatalyst, the photocatalytic performance of Cu_2O remains suboptimal owing to the large size of most Cu_2O photocatalysts synthesized to date (typically tens to hundreds of nanometers). Accordingly, surface active sites needed for N_2 adsorption are limited, whilst bulk recombination consumes a high percentage of photogenerated electrons and holes,[8] severely restricting the photocatalytic activity of Cu_2O for N_2 fixation. Ultrafine nanostructured photocatalysts with lateral size of less than 10 nm offer a promising approach for addressing the aforementioned challenges,[9] due to the ~1 order-of-magnitude increase in exposed surface sites relative to conventional nanoparticle photocatalysts and improved charge migration efficiency.[10] These attributes allow very efficient conversion of reactant molecules.[11] By analogy, the design and synthesis of ultrafine Cu_2O represent a prudent strategy for improving the photocatalytic activity of Cu_2O for pNRR.[12] Whilst ultrafine Cu_2O would potentially deliver superior pNRR activity, the direct synthesis of ultrafine Cu_2O has proved challenging to date.[13] Discovering a reliable synthetic strategy towards ultrafine Cu_2O represents a prized research target.

Freestanding Cu_2O nanocrystals with defined shapes and sizes have previously been prepared through the direct oxidation of metallic Cu nanoparticles or the reduction of self-assembled Cu(II)-containing nanomaterials.[14] However, reports of the synthesis of well-dispersive Cu_2O nanocrystals with a size below 50 nm are rare.[13a, 15] To realize ultrafine Cu_2O, it is generally necessary to prepare Cu_2O by direct growth on a support,[16] a procedure which demands precise control of the addition of the Cu precursor and reaction conditions. For instance, 10 nm Cu_2O particles assembled on BiOBr nanoplates were obtained using ethylene diamine tetraacetic acid and cetyltrimethyl ammonium bromide as capping agents. Further, some 5 nm Cu_2O particles were grown onto graphene-based supports.[17] A facile route for the synthesis of ultrafine Cu_2O with lateral size below 5 nm (even less than 3 nm) under ambient conditions has yet to be reported.

Layered double hydroxide (LDH) is a family of two-dimensional layered clays. Over the past 5 years, LDHs have been extensively studied as catalyst supports or catalyst precursors owing to their tunable divalent and trivalent cation composition and their ability to undergo topotactic transformations with heating.[18] Cu(II)-containing ternary LDHs, incorporating $Cu(OH)_6$ units in the layered 2D sheets composed of MO_6 octahedra, serve as tantalizing precursors for the preparation of ultrafine Cu_2O *via* the *in-situ* reduction of Cu(II) species using mild reducing agents.[19] Here, only Cu^{2+} cations in the host layers are reduced, whilst the remaining divalent and trivalent metal cations are unaffected thus preserving the basic LDH structure. We postulated that through this strategy it should be possible to obtain ultrafine Cu_2O due to the high dispersity of Cu^{2+} ions in the host layers and the spatial confinement of any formed Cu_2O (the latter being especially important for which suppressing Cu_2O excessive grain growth and agglomeration which prevents the synthesis of freestanding ultrafine Cu_2O).[20] Moreover, the LDH support will ensure that the ultrafine Cu_2O generated will have good dispersibility in the aqueous reaction medium used for pNRR.[21] Combining intrinsic properties of Cu_2O with structural advantages of ultrafine photocatalysts, we hypothesized that supported ultrafine Cu_2O prepared by *in-situ* reduction of a Cu(II)-containing LDH should offer excellent pNRR performance compared to conventional bulk Cu_2O photocatalysts with large particle sizes and most of NRR photocatalysts reported. Experimental work presented below validated this hypothesis.

In this work, we describe the successful synthesis of sub-3 nm ultrafine Cu_2O by the *in-situ* topotactic transformation (controlled reduction) of CuZnAl-LDH (denoted here as LDH) nanosheets (Scheme 1), which represents one of the finest Cu_2O synthesized to date. The ultrafine Cu_2O was obtained *via* a mild reduction process at ambient temperature, which used ascorbic acid as the reducing agent. The evolution of ultrafine Cu_2O was controlled by varying the concentration of ascorbic acid and the reduction time. The obtained LDH-supported ultrafine Cu_2O was applied to photocatalytic reduction of N_2 to NH_3 for the first time, exhibiting superior pNRR activity compared with supported bulk Cu_2O nanocrystals of larger size and most of pNRR photocatalysts reported recently (the ultrafine Cu_2O afforded a visible light-driven pNRR activity of 4.10 mmol $g_{Cu_2O}^{-1}$ h^{-1}, ~64 times higher than a bulk Cu_2O reference photocatalyst). Advanced spectroscopic characterization studies, including time-resolved photoluminescence spectra (TPL) and time-resolved absorption spectroscopy (TAS) analysis, allowed the enhanced photocatalytic performance of the sub-3 nm ultrafine Cu_2O to be rationalized in terms of the generation of long-lived photo-excited electrons and highly exposed surface sites for N_2 adsorption and activation.

Results and Discussion

Scheme 1. Synthetic strategy used to prepare LDH-supported sub-3 nm ultrafine Cu_2O.

A one-step *in-situ* reduction approach, using ascorbic acid as the reducing agent, was applied to the synthesis of supported ultrafine Cu_2O from ternary metal LDH precursor. The morphology of the partially reduced sample (denoted herein as u-Cu_2O-0.05M-2h) was first investigated. High-resolution transmission electron microscopy (HRTEM) showed the uniform dispersion of ultrafine Cu_2O particles (black dots) with an average size of 2.22 nm on the LDH nanosheets (Figure 1a-c), which was one of the finest Cu_2O synthesized to date. Closer observation with HRTEM (Figure 1b) revealed lattice fringes with a d-spacing of 0.246 nm, which could readily be assigned to the (111) plane of cubic-phase

10.1002/anie.202013594

Cu_2O, in good agreement with the X-ray diffraction (XRD) patterns for the same sample (Figure S1a-b). Results indicate the successful synthesis of ultrafine Cu_2O with the general preservation of the LDH structure after the mild ascorbic acid reduction process. Atomic force microscopy (AFM) (Figure 1d-e) revealed that the u-Cu_2O-0.05M-2h possessed a relatively uniform thickness (~4.83 nm), with energy-dispersive X-ray spectroscopy (EDS) mapping (Figure 1f) showing a homogeneous distribution of metal elements within the sample suggesting that the LDH structure was largely maintained with ultrafine Cu_2O formation.

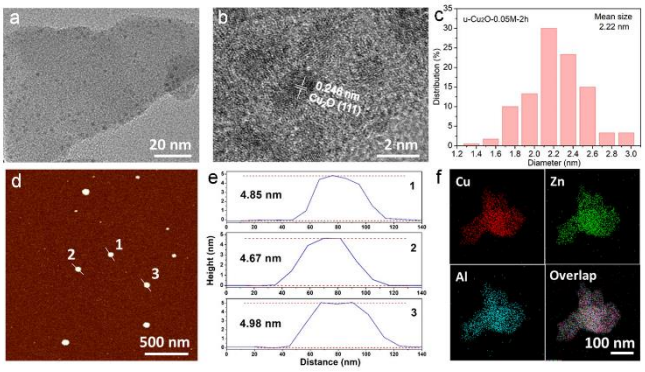

Figure 1. (a-b) HRTEM images at different magnifications of u-Cu_2O-0.05M-2h and (c) the corresponding size distribution histogram. (d) AFM image and (e) AFM height profiles of u-Cu_2O-0.05M-2h (the numbers 1 to 3 in (d) correspond to the profiles 1 to 3 in (e)). (f) EDS element maps for u-Cu_2O-0.05M-2h.

To explore the evolution of ultrafine Cu_2O during the *in-situ* reduction process, the effects of ascorbic acid concentration and ascorbic acid reduction time were systematically studied. Samples obtained by reacting LDH with 0.05 mol L^{-1} of ascorbic acid for different times (t = 0.2, 0.5, 1, 2, or 3 h) are denoted herein as u-Cu_2O-0.05M-t. As shown in the UV-vis diffuse reflectance spectra (UV-DRS) of Figure S1c, the absorption peak at around 475 nm associated with Cu_2O intensified with reduction time up to 2 h, but showed no further noticeable change on increasing the reduction time to 3 h.[13a, 14a] Results suggested that the formation and growth of ultrafine Cu_2O were completed within 2 h. This was further studied by capturing the morphological evolution of ultrafine Cu_2O (Figure S2). The HRTEM images showed that ultrafine Cu_2O with a mean size of ~2.20 nm emerged after only 0.2 h, thereafter the yield of ultrafine Cu_2O increased and approached a maximum after 2 h, implying reaction completion had been achieved.[22] To summarize, ultrafine Cu_2O formed continuously for a specific period of time from LDH, whilst maintaining a sub-3 nm of particle size. The size control was likely due to the spatial confinement of Cu_2O by the LDH laminate structure.[20a, 23]

Next, the effect of ascorbic acid concentration was explored, using a fixed *in-situ* reduction time of 2 h. Samples were synthesized using ascorbic acid concentrations of 0.01, 0.05, 0.5 mol L^{-1}, with the resulting samples being denoted herein as u-Cu_2O-c-2h (i.e. u-Cu_2O-0.01M-2h, u-Cu_2O-0.05M-2h and u-Cu_2O-0.5M-2h, respectively), as depicted graphically in Figure 2a. HRTEM (Figure 2a) indicated that the density and size of the ultrafine Cu_2O on the nanosheets followed the sequence: u-Cu_2O-0.5M-2h (2.66 nm) > u-Cu_2O-0.05M-2h (2.22 nm) > u-Cu_2O-0.01M-2h (1.99 nm), with the corresponding size distributions shown in Figure 1c and Figure S3a-b. To better underline the advantages of ultrafine Cu_2O, bulk Cu_2O with an average size of 61.01 nm and bulk Cu_2O grafted onto LDH nanosheets were prepared as control samples (these denoted herein as b-Cu_2O and b-Cu_2O/LDH, respectively).[13a] TEM, size distributions and XRD for the control samples were presented in Figure S3c-d and S4-S5. Detailed examination of the XRD patterns (Figure 2b) for u-Cu_2O-c-2h showed that the intensity of Cu_2O (111) diffraction peak increased with ascorbic acid concentration, following the order u-Cu_2O-0.01M-2h < u-Cu_2O-0.05M-2h < u-Cu_2O-0.5M-2h, suggestive of a corresponding increase in the concentration of ultrafine Cu_2O.[24] The optical properties of u-Cu_2O-c-2h and bulk counterparts were investigated by UV-DRS (Figure 2c). The u-Cu_2O-c-2h showed three absorption peaks: (1) a band at 200-318 nm due to the intrinsic absorption of LDH involving the ligand-metal and metal-metal charge transfer;[25] (2) an absorption peak around 800 nm associated with $^2E_g \rightarrow {}^2T_{2g}$ (D) d-d transitions of Cu^{2+} ions in LDH;[26] and (3) an absorption feature at ~475 nm associated with ultrafine Cu_2O which intensified in the order u-Cu_2O-0.01M-2h < u-Cu_2O-0.05M-2h < u-Cu_2O-0.5M-2h. Both b-Cu_2O and b-Cu_2O/LDH showed similar absorption signals in the 200-600 nm range (Figure 2c and S6). Cu K-edge X-ray absorption near-edge spectroscopy (XANES) was used to examine the local structure of Cu atoms in the ultrafine Cu_2O and bulk Cu_2O reference samples (Figure 2d and S7). The pre-edge feature at around 8983.8 eV was assigned to a 1s→4p transition of a Cu(I) species, with the intensity of this spectral feature increasing in the order u-Cu_2O-0.01M-2h < u-Cu_2O-0.05M-2h < u-Cu_2O-0.5M-2h.[27] The amounts of ultrafine Cu_2O loaded were further determined by inductively coupled plasma tests on the basis of "coordinating etching" strategy (Table S1). Results again demonstrated that the amount of sub-3 nm ultrafine Cu_2O was dependent on the ascorbic acid concentration used in the *in-situ* reduction process, consistent with the earlier HRTEM, XRD, UV-DRS and XANES findings. By tuning concentration of ultrafine Cu_2O, the sub-3 nm ultrafine Cu_2O with the optimized exposed surface sites along with the favorable light absorption was anticipated to dramatically expedite the photocatalytic ammonia synthesis of Cu_2O.

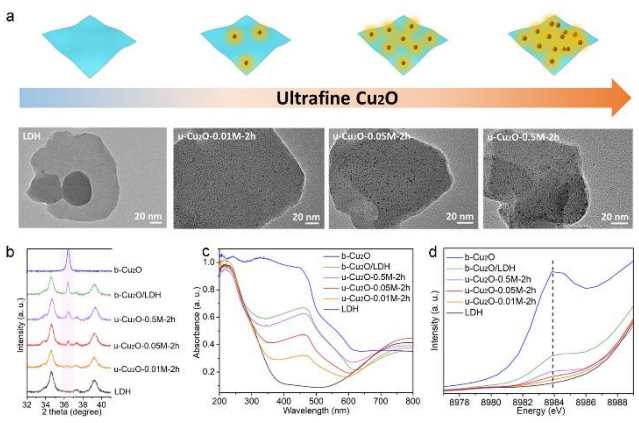

Figure 2. (a) Schematic illustration and HRTEM images of the supported ultrafine Cu_2O prepared through *in-situ* reduction of LDH using different concentrations of ascorbic acid. (b) XRD patterns from 2θ = 32-41° for different samples. The Cu_2O (111) reflection is highlighted. (c) UV-DRS spectra and (d) Cu K-edge XANES spectra for LDH, u-Cu_2O-c-2h (X = 0.01, 0.05 and 0.5 M), b-Cu_2O and b-Cu_2O/LDH.

10.1002/anie.202013594

To ascertain the merits of ultrafine Cu_2O for pNRR, we tested the performance of the u-Cu_2O-c-2h (c = 0.01, 0.05 and 0.5 M) against bulk Cu_2O (b-Cu_2O and b-Cu_2O/LDH) and pristine LDH in the N_2-saturated water (without sacrificial agents) under visible light irradiation, using rigorous detection methods for product quantification. As shown in Figure 3a, all the samples except LDH were active for photocatalytic N_2 reduction indicating that Cu_2O was the light-absorbing/active species responsible for pNRR. Photons absorbed by LDH in the visible light region (involving d-d transitions of the Cu^{2+} ions) could not be utilized to drive pNRR. The rates of NH_3 generation followed the trend of: u-Cu_2O-0.05M-2h (30.31 μmol g^{-1} h^{-1}) > u-Cu_2O-0.01M-2h (22.01 μmol g^{-1} h^{-1}) > u-Cu_2O-0.5M-2h (18.67 μmol g^{-1} h^{-1}) > b-Cu_2O (3.04 μmol g^{-1} h^{-1}) > b-Cu_2O/LDH (1.29 μmol g^{-1} h^{-1}) > LDH (trace). Significantly, the Cu_2O-mass-normalized NH_3 production rate of u-Cu_2O-0.05M-2h can reach to 4.10 mmol $g_{Cu_2O}^{-1}$ h^{-1}, which is superior to most of benchmark photocatalysts reported (Table S2), indicating an outstanding photocatalytic activity and atomic utilization of sub-3 nm ultrafine Cu_2O. Again, u-Cu_2O-0.05M-2h afforded the highest NH_3 generation rate normalized with specific surface area (0.78 μmol m^{-2} h^{-1}), compared to the other ultrafine Cu_2O and bulk Cu_2O photocatalysts (Figure S8-S9). The lower than expected photocatalytic activity of u-Cu_2O-0.5M-2h was likely due to ultrafine Cu_2O aggregation during the tests, thus decreasing the availability of ultrafine Cu_2O. Further time-dependent pNRR experiments were performed for u-Cu_2O-0.05M-2h (Figure 3b), alongside rigorous blank experiments. The amount of NH_3 generated increased almost linearly with the visible light irradiation time, confirmed by ion chromatography data for NH_4^+ quantification (Figure S10). Negligible amounts of NH_3 were produced when N_2 was replaced with Ar under visible light irradiation, or when experiments were conducted with N_2 in the dark. Results provided strong evidence that ultrafine Cu_2O was able to photocatalytic convert N_2 to NH_3. Further, isotope labeling experiments were performed using $^{15}N_2$ with the indophenol product containing ^{15}N detected at m/z 199.05 (Figure S11), which unambiguously confirmed that the NH_3 detected in this current study originated from N_2 photofixation, rather than some other nitrogen source. Moreover, the u-Cu_2O-0.05M-2h was structurally robust and photocatalytically stable, as evidenced by a negligible change in activity, morphology or physico-chemical properties during pNRR cycling tests (Figure 3c, S12-S14). As shown in Figures S15-S17, in addition to O_2, other potential by-products (including NO_3^-, N_2H_4 and H_2) were not detected during the pNRR experiments, indicating the high selectivity of the ultrafine Cu_2O for NH_3 synthesis. To determine the apparent quantum efficiency (QE) of pNRR over u-Cu_2O-0.05M-2h, we performed photocatalytic N_2 reduction experiments under different monochromatic light irradiation (400, 450, 500, 550, 600, 650, and 700 nm) (Figure 3d). Monochromatic light of wavelengths 400 and 450 nm afforded the best N_2 photoreduction activity with QEs of 0.14% and 0.11%, respectively. u-Cu_2O-0.05M-2h demonstrated almost no photocatalytic activity for N_2 reduction under monochromatic light of wavelengths 700 nm (a wavelength outside the absorption range of Cu_2O).

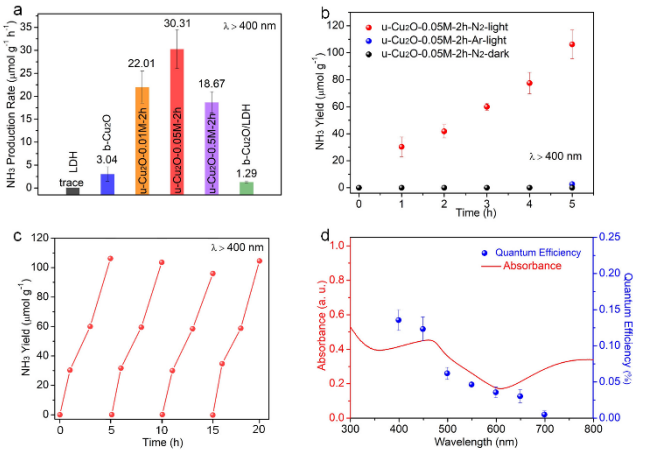

Figure 3. (a) Photocatalytic NH_3 production rate for LDH, u-Cu_2O-c-2h (c = 0.01, 0.05 and 0.5 M), b-Cu_2O and b-Cu_2O/LDH in N_2-saturated water under 1 h visible light irradiation. (b) Time course study of photocatalytic N_2 reduction and various control experiments over u-Cu_2O-0.05M-2h. (c) pNRR cycling test data for photocatalytic N_2 reduction over u-Cu_2O-0.05M-2h. (d) Wavelength-dependent apparent QE for N_2 photoreduction over u-Cu_2O-0.05M-2h.

To gain a deep understanding of the factors contributing to the enhanced pNRR activity of ultrafine Cu_2O, we examined three principal properties that underpin efficient photocatalytic processes: (i) the generation of photo-excited charge carriers by light absorption; (ii) the separation and transfer of photo-excited charge carriers to the surface; (iii) the charge carriers participating in surface catalytic reactions.[28] u-Cu_2O-0.05M-2h and b-Cu_2O/LDH were selected as representative examples of ultrafine Cu_2O and bulk Cu_2O, respectively, thus allowing the particular advantages of ultrafine Cu_2O to be gauged. From the analysis of UV-DRS spectra (Figure 2c), the b-Cu_2O/LDH showed stronger visible-light absorption (400-650 nm) than u-Cu_2O-0.05M-2h, but much worse pNRR performance. It can thus be concluded that the light absorption capacity was not a key factor for the enhanced pNRR activity of u-Cu_2O-0.05M-2h. Charge separation and charge transfer efficiencies following photoexcitation are known to play an important role in overall photocatalytic performance. Electrochemical impedance spectra (EIS) and transient photocurrent (TPC) response measurements were therefore carried out. u-Cu_2O-0.05M-2h offered a more depressed semicircle in the Nyquist plot (lower interfacial charge transfer resistance) and a higher TPC density (Figure 4a) compared to b-Cu_2O/LDH, indicating that charge separation and transport were more efficient in u-Cu_2O-0.05M-2h. Moreover, TPL spectroscopic experiments (Figure 4b) revealed that the short (τ1), long (τ2) and average decay time (τ) were all longer in u-Cu_2O-0.05M-2h compared with b-Cu_2O/LDH, providing solid evidence that ultrafine Cu_2O could effectively inhibit charge carrier recombination (thus increasing the availability of charges for surface photoreactions). The presence of the long-lived charge carriers in u-Cu_2O-0.05M-2h motivated a detailed investigation of charge carrier kinetics in the photocatalyst.

Femtosecond TAS kinetics analysis data for u-Cu_2O-0.05M-2h were presented in Figure 4c-d. A pump-probe configuration equipped with pump laser (480 nm) and infrared continuum probe was adopted here for TAS measurements. The pump laser was used to excite electrons from the valence band (VB) to conduction band (CB). Initially, u-Cu_2O-0.05M-2h exhibited a more protracted

10.1002/anie.202013594

build-up process ($\tau_{build\text{-}up}$ = 444 ± 33 fs) compared with b-Cu_2O/LDH ($\tau_{build\text{-}up}$ = 131 ± 18 fs). Such a sub-picosecond build-up process reflects intraband relaxation (or cooling down processes) arising from electron-phonon coupling in the photo-excited Cu_2O.[29] Fitting the subsequent biexponential decay curve yielded $\tau1$ = 5.35 ± 0.65 ps and $\tau2$ = 47.16 ± 8.99 ps for u-Cu_2O-0.05M-2h, and $\tau1$ = 3.02 ± 0.16 ps and $\tau2$ = 18.73 ± 2.45 ps for b-Cu_2O/LDH. Using ultrafine Cu_2O therefore increased $\tau1$ and $\tau2$ by ~1.8 and 2.5 times, respectively, compared to the bulk Cu_2O counterpart. These two relaxation processes ($\tau1$ and $\tau2$) resulted from photo-excited electron relaxation mediated by rich trap states, with such states being in abundance in the ultrafine Cu_2O.[30] In brief, the fast decay component $\tau1$ arises from the trapping of electrons from the CB into trap states within the bandgap, whilst the much slower decay component $\tau2$ is due to recombination processes involving CB electrons/trapped electrons and VB holes.[31] Considering the above data, the superior pNRR activity of u-Cu_2O-0.05M-2h can be rationalized. The sub-3 nm ultrafine Cu_2O possesses an abundance of trap states that are efficient in capturing photo-excited electrons (thus suppressing electron-hole recombination), with the ultrafine size of u-Cu_2O-0.05M-2h benefitting the multi-electron-transfer processes involved in surface N_2 reduction to NH_3.

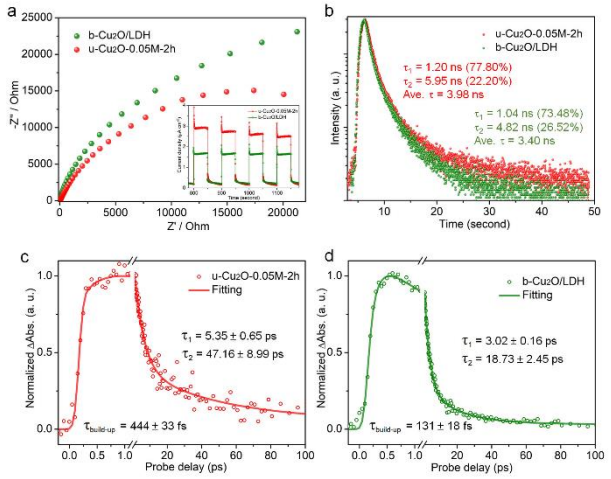

Figure 4. (a) EIS Nyquist plots for u-Cu_2O-0.05M-2h and b-Cu_2O/LDH (the inset shows the periodic on/off TPC response). (b) TPL decay curves for u-Cu_2O-0.05M-2h and b-Cu_2O/LDH. TAS kinetics analysis for (c) u-Cu_2O-0.05M-2h and (d) b-Cu_2O/LDH.

The final step in the pNRR process is catalytic redox reactions on the surface of ultrafine Cu_2O, which encompasses the adsorption of N_2 and its reduction by photo-excited electrons. N_2 adsorption is an important prerequisite in pNRR.[32] Sub-3 nm ultrafine Cu_2O with highly exposed surface sites was expected to enhance N_2 adsorption. This was confirmed by the experiment (Figure S19), where the ultrafine Cu_2O sample offered a higher N_2 adsorption capacity than its bulk Cu_2O counterpart. Subsequently, the photo-excited electron transfer pathway was probed. From the Tauc analyses (Figure S20), the bandgaps for Cu_2O and LDH were estimated to be ~2.03 and 3.08 eV, respectively. Thus, it would be reasonable to infer that upon visible light irradiation of U-Cu_2O-2, only Cu_2O would be photoexcited to generate electrons and holes for surface redox reactions, with the underlying LDH simply serving as a structural support in the pNRR process.[33] This coincides with what was observed in the photo-deposition experiments (Figure S21), Pt and Au nanoparticles formed next to the ultrafine Cu_2O (i.e. the reduction of Pt^{2+} to Pt^0 or Au^{3+} to Au^0 would preferentially occur in the vicinity of Cu_2O rather than on the exposed LDH nanosheets), thus confirming simultaneously that ultrafine Cu_2O acted as the light absorption unit and active species for pNRR.[8a, 34] The reduction potentials of N_2 on u-Cu_2O-0.05M-2h and b-Cu_2O/LDH were determined from electrochemical measurements (Figure S22). A much higher current density was observed for u-Cu_2O-0.05M-2h in N_2-saturated solution compared with an Ar-saturated solution, confirming u-Cu_2O-0.05M-2h was indeed active for N_2 reduction.[35] Compared with the bulk Cu_2O, the onset potential for N_2 reduction over ultrafine Cu_2O was shifted to positive potentials, along with a markedly enhanced current density. Results suggested that the supported ultrafine Cu_2O enhanced pNRR activity by lowering the energy barrier for N_2 reduction.[36]

Conclusion

In summary, sub-3 nm ultrafine Cu_2O was successfully synthesized by the partial reduction of a CuZnAl-LDH precursor with ascorbic acid at room temperature and was exploited to efficient photocatalytic reduction of N_2 to NH_3 for the first time. The density of the ultrafine Cu_2O on the surface of LDH support could be controlled by varying the concentration of the ascorbic acid or the reduction time. Reducing the lateral dimensions of Cu_2O to less than 3 nm endowed the ultrafine Cu_2O with highly exposed surface sites for N_2 adsorption and ample trap states for long-lived electrons, attributes that were both highly beneficial for the photocatalytic N_2 reduction to NH_3 under visible light irradiation. The introduction of a new family of Cu_2O photocatalysts open up new opportunities for photocatalytic N_2 fixation and the facile route described here for the creation of ultrafine Cu_2O from a LDH precursor is expected to be widely adopted in the future by other researchers for the synthesis of high-performance Cu_2O-based catalysts.

Acknowledgements

The authors are grateful for financial support from the National Key Projects for Fundamental Research and Development of China (2018YFB1502002, 2017YFA0206904, 2017YFA0206900, 2018YFA0208701), the National Natural Science Foundation of China (51825205, 51772305, 52072382, 21871279, 21802154, 21902168, 21633015, 11721404), the Beijing Natural Science Foundation (2191002, 2182078, 2194089), the Strategic Priority Research Program of the Chinese Academy of Sciences (XDB17000000), the Royal Society Newton Advanced Fellowship (NA170422), the International Partnership Program of Chinese Academy of Sciences (GJHZ1819, GJHZ201974), the K. C. Wong Education Foundation, and the Youth Innovation Promotion Association of the CAS. The XAFS experiments were conducted in 1W1B beamline of Beijing Synchrotron Radiation Facility (BSRF). The isotopic labeling experiments were conducted in BioNMR facility, Tsinghua University Branch of China National Center for Protein Sciences (Beijing). GINW acknowledges

funding support from the Energy Education Trust of New Zealand, the MacDiarmid Institute for Advanced Materials and Nanotechnology and the Dodd Walls Centre for Photonic and Quantum Technologies.

Keywords: ultrafine Cu_2O • photocatalysis • nitrogen fixation • visible light.

[1] a) S. Zhang, Y. Zhao, R. Shi, G. I. N. Waterhouse, T. Zhang, *EnergyChem* **2019**, *1*, 100013; b) S. Y. Wang, F. Ichihara, H. Pang, H. Chen, J. H. Ye, *Adv. Funct. Mater.* **2018**, *28*, 1803309.

[2] a) H. Li, J. Shang, Z. Ai, L. Zhang, *J. Am. Chem. Soc.* **2015**, *137*, 6393-6399; b) A. J. Medford, M. C. Hatzell, *ACS Catal.* **2017**, *7*, 2624-2643.

[3] a) Y. Liu, M. Cheng, Z. He, B. Gu, C. Xiao, T. Zhou, Z. Guo, J. Liu, H. He, B. Ye, B. Pan, Y. Xie, *Angew. Chem. Int. Ed.* **2019**, *58*, 731-735; b) N. Zhang, A. Jalil, D. Wu, S. Chen, Y. Liu, C. Gao, W. Ye, Z. Qi, H. Ju, C. Wang, X. Wu, L. Song, J. Zhu, Y. Xiong, *J. Am. Chem. Soc.* **2018**, *140*, 9434-9443.

[4] H. Li, C. Mao, H. Shang, Z. Yang, Z. Ai, L. Zhang, *Nanoscale* **2018**, *10*, 15429-15435.

[5] X. Chen, N. Li, Z. Kong, W.-J. Ong, X. Zhao, *Mater. Horiz.* **2018**, *5*, 9-27.

[6] a) S. Paria, O. Reiser, *ChemCatChem* **2014**, *6*, 2477-2483; b) J. Cui, U. J. Gibson, *J. Phys. Chem. C* **2010**, *114*, 6408-6412.

[7] a) L. Wan, Q. Zhou, X. Wang, T. E. Wood, L. Wang, P. N. Duchesne, J. Guo, X. Yan, M. Xia, Y. F. Li, A. A. Jelle, U. Ulmer, J. Jia, T. Li, W. Sun, G. A. Ozin, *Nat. Catal.* **2019**, *2*, 889-898; b) X. Chang, T. Wang, Z.-J. Zhao, P. Yang, J. Greeley, R. Mu, G. Zhang, Z. Gong, Z. Luo, J. Chen, Y. Cui, G. A. Ozin, J. Gong, *Angew. Chem. Int. Ed.* **2018**, *57*, 15415-15419; c) A. D. Handoko, J. Tang, *Int. J. Hydrogen Energy* **2013**, *38*, 13017-13022.

[8] a) L. Wang, J. Ge, A. Wang, M. Deng, X. Wang, S. Bai, R. Li, J. Jiang, Q. Zhang, Y. Luo, Y. Xiong, *Angew. Chem. Int. Ed.* **2014**, *53*, 5107-5111; b) X. Yuan, H. Yuan, L. Ye, J. Hu, Y. Xu, P. Li, *RSC Adv.* **2015**, *5*, 42855-42860.

[9] a) Y. Sun, S. Gao, F. Lei, C. Xiao, Y. Xie, *Acc. Chem. Res.* **2015**, *48*, 3-12; b) C. Tan, X. Cao, X.-J. Wu, Q. He, J. Yang, X. Zhang, J. Chen, W. Zhao, S. Han, G.-H. Nam, M. Sindoro, H. Zhang, *Chem. Rev.* **2017**, *117*, 6225-6331.

[10] a) Z. Li, S. Ji, Y. Liu, X. Cao, S. Tian, Y. Chen, Z. Niu, Y. Li, *Chem. Rev.* **2020**, *120*, 623-682; b) S. Hu, X. Wang, *Chem. Soc. Rev.* **2013**, *42*, 5577-5594.

[11] a) H.-L. Wu, X.-B. Li, C.-H. Tung, L.-Z. Wu, *Adv. Mater.* **2019**, *31*, 1900709; b) Y. Sun, S. Gao, F. Lei, Y. Xie, *Chem. Soc. Rev.* **2015**, *44*, 623-636.

[12] a) I. Chakraborty, T. Pradeep, *Chem. Rev.* **2017**, *117*, 8208-8271; b) H. Zhang, P. Zhang, M. Qiu, J. Dong, Y. Zhang, X. W. Lou, *Adv. Mater.* **2019**, *31*, 1804883; c) J. Lin, Y. Shang, X. Li, J. Yu, X. Wang, L. Guo, *Adv. Mater.* **2017**, *29*, 1604797.

[13] a) W.-H. Ke, C.-F. Hsia, Y.-J. Chen, M. H. Huang, *Small* **2016**, *12*, 3530-3534; b) M. Yin, C.-K. Wu, Y. Lou, C. Burda, J. T. Koberstein, Y. Zhu, S. O'Brien, *J. Am. Chem. Soc.* **2005**, *127*, 9506-9511.

[14] a) A. Singhal, M. R. Pai, R. Rao, K. T. Pillai, I. Lieberwirth, A. K. Tyagi, *Eur. J. Inorg. Chem.* **2013**, *2013*, 2640-2651; b) L.-I. Hung, C.-K. Tsung, W. Huang, P. Yang, *Adv. Mater.* **2010**, *22*, 1910-1914; c) J. J. Teo, Y. Chang, H. C. Zeng, *Langmuir* **2006**, *22*, 7369-7377.

[15] C.-H. Kuo, M. H. Huang, *Nano Today* **2010**, *5*, 106-116.

[16] a) W. Cui, W. An, L. Liu, J. Hu, Y. Liang, *J. Hazard. Mater.* **2014**, *280*, 417-427; b) Y. Zhou, G. Liu, X. Zhu, Y. Guo, *Ceram. Int.* **2017**, *43*, 8372-8377; c) M. Cabrero-Antonino, S. Remiro-Buenamañana, M. Souto, A. A. García-Valdivia, D. Choquesillo-Lazarte, S. Navalón, A. Rodríguez-Diéguez, G. Mínguez Espallargas, H. García, *Chem. Commun.* **2019**, *55*, 10932-10935.

[17] a) L. Liu, X. Gu, C. Sun, H. Li, Y. Deng, F. Gao, L. Dong, *Nanoscale* **2012**, *4*, 6351-6359; b) J. Chen, S. Shen, P. Guo, M. Wang, P. Wu, X. Wang, L. Guo, *Appl. Catal. B: Environ.* **2014**, *152-153*, 335-341.

[18] Y. Zhao, X. Jia, G. I. N. Waterhouse, L.-Z. Wu, C.-H. Tung, D. O'Hare, T. Zhang, *Adv. Energy Mater.* **2016**, *6*, 1501974.

[19] a) H. Xu, W. Wang, W. Zhu, *J. Phys. Chem. B* **2006**, *110*, 13829-13834; b) J. Ma, J. Ding, L. Li, J. Zou, Y. Kong, S. Komarneni, *Ceram. Int.* **2015**, *41*, 3191-3196.

[20] a) G. Fan, F. Li, D. G. Evans, X. Duan, *Chem. Soc. Rev.* **2014**, *43*, 7040-7066; b) Q. Wang, D. O'Hare, *Chem. Rev.* **2012**, *112*, 4124-4155.

[21] J. Feng, Y. He, Y. Liu, Y. Du, D. Li, *Chem. Soc. Rev.* **2015**, *44*, 5291-5319.

[22] Y. Shi, Z. Lyu, M. Zhao, R. Chen, Q. N. Nguyen, Y. Xia, *Chem. Rev.* **2020**, DOI: 10.1021/acs.chemrev.0c00454.

[23] Y. Xia, P. Yang, Y. Sun, Y. Wu, B. Mayers, B. Gates, Y. Yin, F. Kim, H. Yan, *Adv. Mater.* **2003**, *15*, 353-389.

[24] C. R. Hubbard, R. L. Snyder, *Powder Diffr.* **2013**, *3*, 74-77.

[25] a) N. Baliarsingh, L. Mohapatra, K. Parida, *J. Mater. Chem. A* **2013**, *1*, 4236-4243; b) R. Nakamura, A. Okamoto, H. Osawa, H. Irie, K. Hashimoto, *J. Am. Chem. Soc.* **2007**, *129*, 9596-9597.

[26] Y. Zhao, Y. Zhao, G. I. N. Waterhouse, L. Zheng, X. Cao, F. Teng, L.-Z. Wu, C.-H. Tung, D. O'Hare, T. Zhang, *Adv. Mater.* **2017**, *29*, 1703828.

[27] J. Zheng, J. Ye, M. A. Ortuño, J. L. Fulton, O. Y. Gutiérrez, D. M. Camaioni, R. K. Motkuri, Z. Li, T. E. Webber, B. L. Mehdi, N. D. Browning, R. L. Penn, O. K. Farha, J. T. Hupp, D. G. Truhlar, C. J. Cramer, J. A. Lercher, *J. Am. Chem. Soc.* **2019**, *141*, 9292-9304.

[28] C. Guo, J. Ran, A. Vasileff, S.-Z. Qiao, *Energy Environ. Sci.* **2018**, *11*, 45-56.

[29] a) H. Wang, S. Jiang, W. Shao, X. Zhang, S. Chen, X. Sun, Q. Zhang, Y. Luo, Y. Xie, *J. Am. Chem. Soc.* **2018**, *140*, 3474-3480; b) Z.-J. Jiang, D. F. Kelley, *J. Phys. Chem. C* **2011**, *115*, 4594-4602.

[30] a) D. A. Wheeler, J. Z. Zhang, *Adv. Mater.* **2013**, *25*, 2878-2896; b) Y. Du, Z. Wang, H. Chen, H.-Y. Wang, G. Liu, Y. Weng, *Phys. Chem. Chem. Phys.* **2019**, *21*, 4349-4358.

[31] a) X. Jiao, Z. Chen, X. Li, Y. Sun, S. Gao, W. Yan, C. Wang, Q. Zhang, Y. Lin, Y. Luo, Y. Xie, *J. Am. Chem. Soc.* **2017**, *139*, 7586-7594; b) Q. Liu, Z. Wang, H. Chen, H.-Y. Wang, H. Song, J. Ye, Y. Weng, *ChemCatChem* **2020**, DOI: 10.1002/cctc.202000280.

[32] a) S. Zhang, Y. Zhao, R. Shi, C. Zhou, G. I. N. Waterhouse, L. Z. Wu, C. H. Tung, T. Zhang, *Adv. Energy Mater.* **2020**, *10*, 1901973; b) H. Hirakawa, M. Hashimoto, Y. Shiraishi, T. Hirai, *J. Am. Chem. Soc.* **2017**, *139*, 10929-10936; c) H. Jia, A. Du, H. Zhang, J. Yang, R. Jiang, J. Wang, C.-y. Zhang, *J. Am. Chem. Soc.* **2019**, *141*, 5083-5086.

[33] Z. Wang, S.-M. Xu, L. Tan, G. Liu, T. Shen, C. Yu, H. Wang, Y. Tao, X. Cao, Y. Zhao, Y.-F. Song, *Appl. Catal. B: Environ.* **2020**, *270*, 118884.

[34] a) M. Wang, Y. Liu, D. Li, J. Tang, W. Huang, *Chin. Chem. Lett.* **2019**, *30*, 985-988; b) H. Gong, Y. Zhang, Y. Cao, M. Luo, Z. Feng, W. Yang, K. Liu, H. Cao, H. Yan, *Appl. Catal. B: Environ.* **2018**, *237*, 309-317.

[35] Y. Shiraishi, M. Hashimoto, K. Chishiro, K. Moriyama, S. Tanaka, T. Hirai, *J. Am. Chem. Soc.* **2020**, *142*, 7574-7583.

[36] a) J. Xie, R. Jin, A. Li, Y. Bi, Q. Ruan, Y. Deng, Y. Zhang, S. Yao, G. Sankar, D. Ma, J. Tang, *Nat. Catal.* **2018**, *1*, 889-896; b) J. Li, S. Chen, F. Quan, G. Zhan, F. Jia, Z. Ai, L. Zhang, *Chem* **2020**, *6*, 885-901.

10.1002/anie.202013594

Entry for the Table of Contents

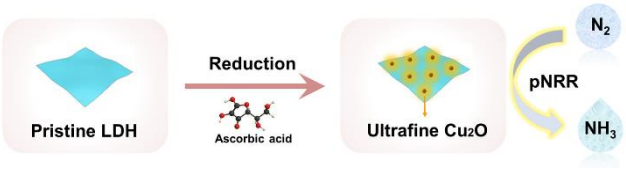

Sub-3 nm ultrafine Cu_2O was synthesized through a facile *in-situ* reduction of LDH, exhibiting superior performance for the visible light-driven N_2 reduction to NH_3, nearly a 64-fold increases in NH_3 production rate compared to bulk Cu_2O and is superior to most of the reported benchmark photocatalysts. The remarkable activity can be attributable to the high availability of surface sites and the generation of long-lived photo-excited electrons.